

Biorthogonal Wavelets with 6-fold Symmetry
for Hexagonal Data and Triangle Surface
Multiresolution Processing

AMS Meeting Special Session, Urbana, IL
March 27-29, 2009

Qingtang Jiang
Dept. of Math and Computer Sci.
University of Missouri–St. Louis
St. Louis, MO 63121, U.S.A.

Outline of the Talk

- Hexagonal sampling
- Triangle surface subdivision
- Biorthogonal wavelets with 6-fold symmetry
- Lifting-scheme-based multiresolution alg.

1 Hexagonal sampling

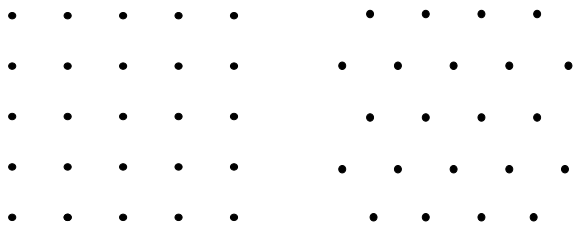


Figure 1: *Left: Rectangular lattice (array); Right: Hexagonal lattice (array)*

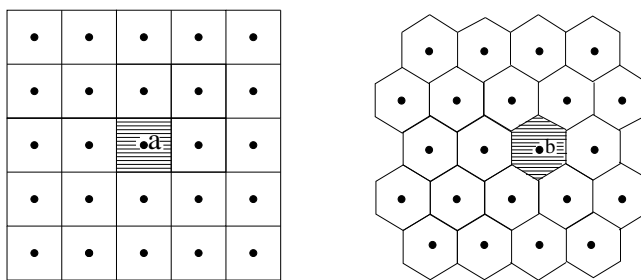
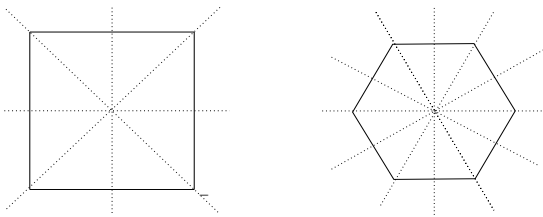


Figure 2: *Left: Square tessellation; Right: Hexagonal tessellation*

Hexagonal lattice

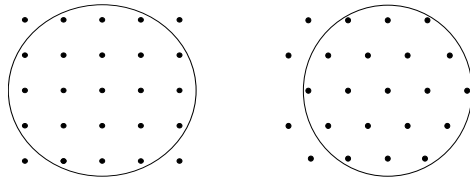
- Fewer sampling points to maintain equally high frequency information
- 6 directional symmetry (while 4-fold symmetry for square lattice)
- Better consistent connectivity
- Orientation banding
- ...
- Pertinent to the vision process

applied in edge detection, pattern recognition, ...
used in Geoscience



$$\text{supp}(\hat{f}) \subset \{\omega \in \mathbb{R}^2 : |\omega| \leq R\}$$

Fewer hexagonal samples needed to recover f .



SMOS (Soil Moisture and Ocean Salinity) mission by European Space Agency

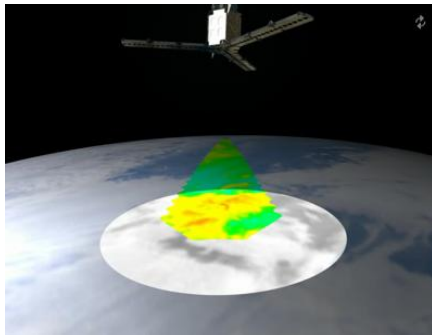


Figure 3: *Y-shaped antenna picks up hexagonally sampled data (picture from Eesa)*

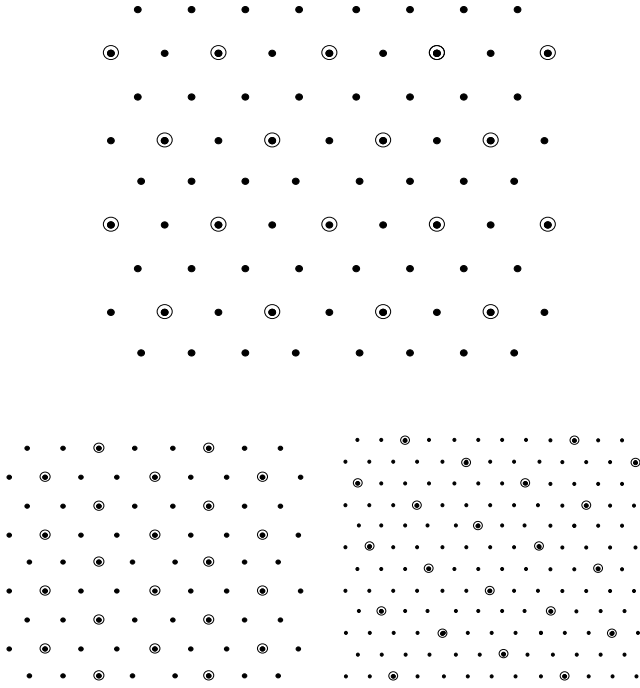


Figure 4: *Top: Dyadic refinement; Bottom: $\sqrt{3}$ and $\sqrt{7}$ refinements*

Highest symmetry may a filter bank $\{p, q^{(1)}, q^{(2)}, q^{(3)}\}$ have?

Regular mesh: (The valence of each vertex is 6).

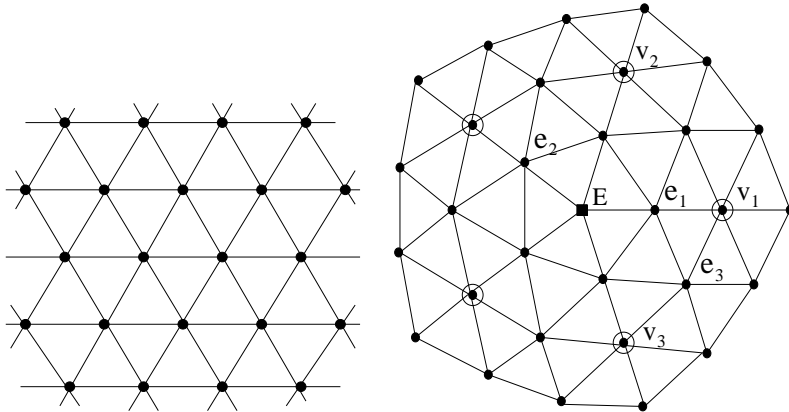


Figure 6: *Left: Regular mesh; Right: Extraordinary vertex E*

e_1, e_2, e_3 have the same algorithm

v_1, v_2, v_3 have the identical algorithm

Rotation and reflection invariant algs.

3 6-fold symmetric biorthogonal wavelets

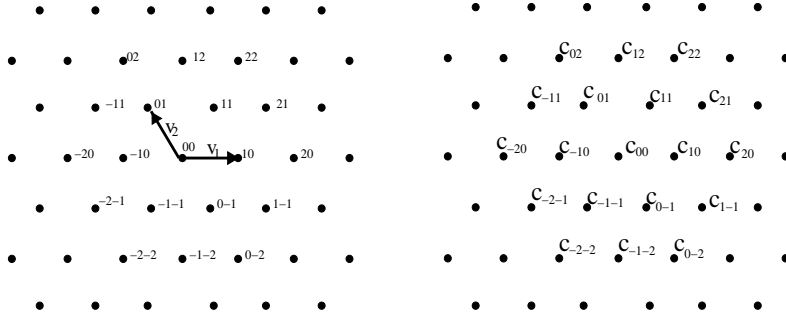


Figure 7: *Left: Indices for hexagonal nodes; Right: Indices for hexagonally sampled data \mathcal{C}*

Decomposition alg. with $\{p, q^{(1)}, q^{(2)}, q^{(3)}\}$:

$$c_{\mathbf{n}}^{j+1} = \frac{1}{4} \sum_{\mathbf{k} \in \mathbf{Z}^2} p_{\mathbf{k}-2\mathbf{n}} c_{\mathbf{k}}^j, \quad d_{\mathbf{n}}^{(\ell, j+1)} = \frac{1}{4} \sum_{\mathbf{k} \in \mathbf{Z}^2} q_{\mathbf{k}-2\mathbf{n}}^{(\ell)} c_{\mathbf{k}}^j,$$

Reconstruction alg. with $\{\tilde{p}, \tilde{q}^{(1)}, \tilde{q}^{(2)}, \tilde{q}^{(3)}\}$:

$$c_{\mathbf{k}}^j = \sum_{\mathbf{n} \in \mathbf{Z}^2} \tilde{p}_{\mathbf{k}-2\mathbf{n}} c_{\mathbf{n}}^{j+1} + \sum_{1 \leq \ell \leq 3} \sum_{\mathbf{n} \in \mathbf{Z}^2} \tilde{q}_{\mathbf{k}-2\mathbf{n}}^{(\ell)} d_{\mathbf{n}}^{(\ell, j+1)}$$

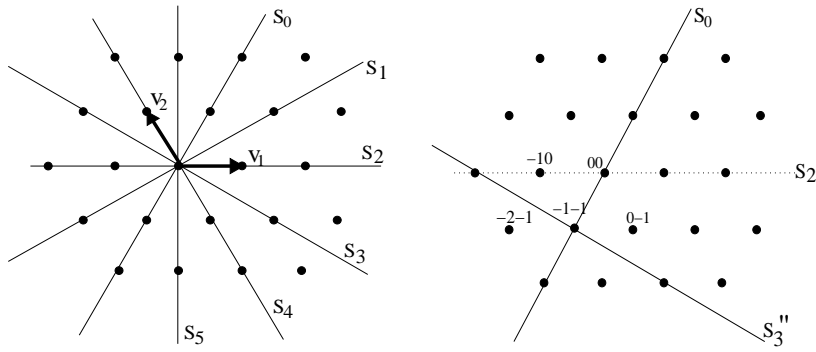


Figure 8: *Left: 6 axes (lines) of symmetry for lowpass filter p ;*
Right: 3 axes (lines) of symmetry for highpass filter $q^{(1)}$

Filter bank $\{p, q^{(1)}, q^{(2)}, q^{(3)}\}$ is said to have **6-fold axial (line) symmetry** if

- (i) lowpass filter $p(\omega)$ is symmetric around S_0, \dots, S_5 ,
- (ii) $e^{-i(\omega_1+\omega_2)}q^{(1)}(\omega)$ is symmetric around the axes S_0, S_3 ,
and
- (iii) $q^{(2)}$ and $q^{(3)}$ are the $\frac{2\pi}{3}$ and $\frac{4\pi}{3}$ rotations of $q^{(1)}$
resp.

For $\{p, q^{(1)}, q^{(2)}, q^{(3)}\}$, with $q^{(0)} = p$, write $q^{(\ell)}(\boldsymbol{\omega})$:

$$q^{(\ell)}(\boldsymbol{\omega}) = \frac{1}{2}(q_0^{(\ell)}(2\boldsymbol{\omega}) + q_1^{(\ell)}(2\boldsymbol{\omega})e^{i(\omega_1+\omega_2)} + q_2^{(\ell)}(2\boldsymbol{\omega})e^{-i\omega_1} + q_3^{(\ell)}(2\boldsymbol{\omega})e^{-i\omega_2}),$$

$q_k^{(\ell)}$ -trigonometric poly. Polyphase matrix $V(\boldsymbol{\omega})$:

$$V(\boldsymbol{\omega}) = \left[q_k^{(\ell)}(\boldsymbol{\omega}) \right]_{0 \leq \ell, k \leq 3}.$$

$$[p, q^{(1)}, q^{(2)}, q^{(3)}]^T(\boldsymbol{\omega}) = \frac{1}{2}V(2\boldsymbol{\omega})I_{00}(\boldsymbol{\omega}),$$

$$I_{00}(\boldsymbol{\omega}) = [1, e^{i(\omega_1+\omega_2)}, e^{-i\omega_1}, e^{-i\omega_2}]^T.$$

Prop. 1 $\{p, q^{(1)}, q^{(2)}, q^{(3)}\}$ has 6-fold axial symmetry iff

$$V(R_1^{-T}\boldsymbol{\omega}) = S_1(\boldsymbol{\omega})V(\boldsymbol{\omega})S_2(\boldsymbol{\omega}),$$

$$V(L_0\boldsymbol{\omega}) = S_0V(\boldsymbol{\omega})S_0,$$

$$S_1(\boldsymbol{\omega}) = \begin{bmatrix} 1 & 0 & 0 & 0 \\ 0 & 0 & 0 & e^{i\omega_2} \\ 0 & e^{-i(\omega_1+\omega_2)} & 0 & 0 \\ 0 & 0 & e^{i\omega_1} & 0 \end{bmatrix}, \quad S_0 = \begin{bmatrix} 1 & 0 & 0 & 0 \\ 0 & 1 & 0 & 0 \\ 0 & 0 & 0 & 1 \\ 0 & 0 & 1 & 0 \end{bmatrix},$$

$$S_2(\boldsymbol{\omega}) = \begin{bmatrix} 1 & 0 & 0 & 0 \\ 0 & 0 & e^{i(\omega_1+\omega_2)} & 0 \\ 0 & 0 & 0 & e^{-i\omega_1} \\ 0 & e^{-i\omega_2} & 0 & 0 \end{bmatrix}.$$

$$L_0 = \begin{bmatrix} 0 & 1 \\ 1 & 0 \end{bmatrix}, \quad R_1 = \begin{bmatrix} 0 & 1 \\ -1 & 1 \end{bmatrix}.$$

Prop. 2 Suppose $\{p, q^{(1)}, q^{(2)}, q^{(3)}\}$ and $\{\tilde{p}, \tilde{q}^{(1)}, \tilde{q}^{(2)}, \tilde{q}^{(3)}\}$ are given by

$$\begin{aligned} [p, q^{(1)}, q^{(2)}, q^{(3)}]^T(\boldsymbol{\omega}) &= V_n(2\boldsymbol{\omega})V_{n-1}(2\boldsymbol{\omega}) \cdots V_0(2\boldsymbol{\omega})I_{00}(\boldsymbol{\omega}), \\ [\tilde{p}, \tilde{q}^{(1)}, \tilde{q}^{(2)}, \tilde{q}^{(3)}]^T(\boldsymbol{\omega}) &= \frac{1}{4}\tilde{V}_n(2\boldsymbol{\omega})\tilde{V}_{n-1}(2\boldsymbol{\omega}) \cdots \tilde{V}_0(2\boldsymbol{\omega})I_{00}(\boldsymbol{\omega}). \end{aligned}$$

Then $\{p, q^{(1)}, q^{(2)}, q^{(3)}\}$ and $\{\tilde{p}, \tilde{q}^{(1)}, \tilde{q}^{(2)}, \tilde{q}^{(3)}\}$ are biorthogonal FIR filter banks with 6-fold symmetry, where $\tilde{V}_j(\boldsymbol{\omega}) = (V_j(\boldsymbol{\omega})^{-1})^*$,

with

$$x = e^{-i\omega_1}, \quad y = e^{-i\omega_2},$$

$$V_j(\boldsymbol{\omega}) = \begin{bmatrix} \gamma + \rho(x + xy + y + \frac{1}{x} + \frac{1}{xy} + \frac{1}{y}) & \alpha(1 + xy) + \beta(x + y) & \alpha(1 + \frac{1}{x}) + \beta(y + \frac{1}{xy}) & \alpha(1 + \frac{1}{y}) + \beta(x + \frac{1}{xy}) \\ \tau(1 + \frac{1}{xy}) & 1 & 0 & 0 \\ \tau(1 + x) & 0 & 1 & 0 \\ \tau(1 + y) & 0 & 0 & 1 \end{bmatrix},$$

$$\rho = \tau(\alpha + 2\beta),$$

$$\tilde{V}_j(\boldsymbol{\omega}) = \frac{1}{\gamma - 6\alpha\tau} \times \begin{bmatrix} 1 & -\tau(1 + xy) & -\tau(1 + \frac{1}{x}) & -\tau(1 + \frac{1}{y}) \\ -(\alpha + \frac{\alpha}{xy} + \frac{\beta}{x} + \frac{\beta}{y}) & \xi(\frac{1}{xy}, y) & \tau(1 + \frac{1}{x})(\alpha + \frac{\alpha}{xy} + \frac{\beta}{x} + \frac{\beta}{y}) & \tau(1 + \frac{1}{y})(\alpha + \frac{\alpha}{xy} + \frac{\beta}{x} + \frac{\beta}{y}) \\ -(\alpha + \alpha x + \beta xy + \frac{\beta}{y}) & \tau(1 + xy)(\alpha + \alpha x + \beta xy + \frac{\beta}{y}) & \xi(x, y) & \tau(1 + \frac{1}{y})(\alpha + \alpha x + \beta xy + \frac{\beta}{y}) \\ -(\alpha + \alpha y + \beta xy + \frac{\beta}{x}) & \tau(1 + xy)(\alpha + \alpha y + \beta xy + \frac{\beta}{x}) & \tau(1 + \frac{1}{x})(\alpha + \alpha y + \beta xy + \frac{\beta}{x}) & \xi(y, x) \end{bmatrix}.$$

6-fold axial symmetric filter banks
yield

algs. with required symmetry for surface multiresolution proc.

4 Lifting-scheme-based multiresolution algorithms

Lifting-scheme-based multiresolution alg. was introduced:

M. Bertram, Biorthogonal Loop-subdivision Wavelets, *Computing*, 72 (2004), 29–39.

works for regular and irregular meshes. But no filter banks, no properties of $\phi, \psi^{(\ell)}, \tilde{\phi}, \tilde{\psi}^{(\ell)}$

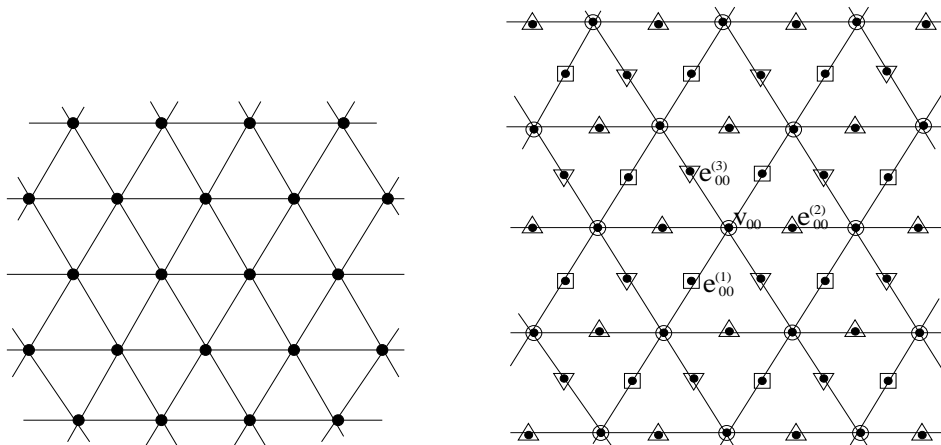


Figure 9: *Left: Regular triangle mesh; Right: Initial data separated into 4 groups: $\{v_{\mathbf{k}}\}, \{e_{\mathbf{k}}^{(1)}\}, \{e_{\mathbf{k}}^{(2)}\}, \{e_{\mathbf{k}}^{(3)}\}$*

$$v_{\mathbf{k}} = c_{2\mathbf{k}}, e_{\mathbf{k}}^{(1)} = c_{2\mathbf{k}-(1,1)}, e_{\mathbf{k}}^{(2)} = c_{2\mathbf{k}+(1,0)}, e_{\mathbf{k}}^{(3)} = c_{2\mathbf{k}+(0,1)}, \mathbf{k} \in \mathbb{Z}^2.$$

Decomposed data:

$\{c_{\mathbf{k}}^1\}_{\mathbf{k}}$ – “approx. part”, $\{d_{\mathbf{k}}^{(\ell,1)}\}_{\mathbf{k}}$, $\ell = 1, 2, 3$ – “details”.

Denote

$$\tilde{v}_{\mathbf{k}} = c_{\mathbf{k}}^1, \tilde{e}_{\mathbf{k}}^{(1)} = d_{\mathbf{k}}^{(1,1)}, \tilde{e}_{\mathbf{k}}^{(2)} = d_{\mathbf{k}}^{(2,1)}, \tilde{e}_{\mathbf{k}}^{(3)} = d_{\mathbf{k}}^{(3,1)}.$$

Associated $\tilde{v}_{\mathbf{k}}, \tilde{e}_{\mathbf{k}}^{(1)}, \tilde{e}_{\mathbf{k}}^{(2)}, \tilde{e}_{\mathbf{k}}^{(3)}$ with

$$2\mathbf{k}, 2\mathbf{k} - (1, 1), 2\mathbf{k} + (1, 0), 2\mathbf{k} + (0, 1).$$

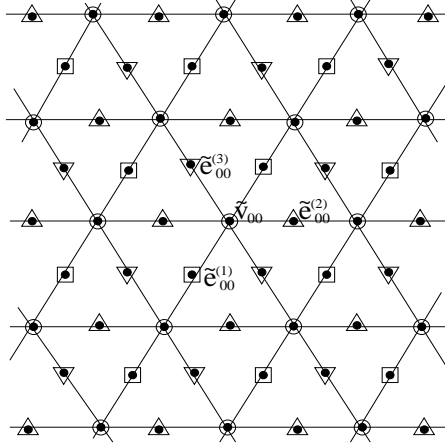


Figure 10: *Decomposed data associated with 4 groups of hexagonal nodes*

Since the same alg. for $\{e_{\mathbf{k}}^{(1)}\}$, $\{e_{\mathbf{k}}^{(2)}\}$, $\{e_{\mathbf{k}}^{(3)}\}$, and
the same alg. for $\{\tilde{e}_{\mathbf{k}}^{(1)}\}$, $\{\tilde{e}_{\mathbf{k}}^{(2)}\}$, $\{\tilde{e}_{\mathbf{k}}^{(3)}\}$,
use e to denote $\{e_{\mathbf{k}}^{(1)}\}$, $\{e_{\mathbf{k}}^{(2)}\}$, $\{e_{\mathbf{k}}^{(3)}\}$,
and \tilde{e} denotes $\{\tilde{e}_{\mathbf{k}}^{(1)}\}$, $\{\tilde{e}_{\mathbf{k}}^{(2)}\}$, $\{\tilde{e}_{\mathbf{k}}^{(3)}\}$.

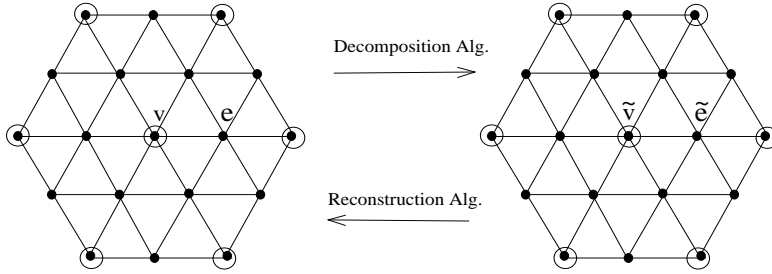


Figure 11: *Decomposition and reconstruction algorithms*

Decomposition Algorithm:

Step 1. $v'' = \frac{1}{b}\{v - d(e_0 + e_1 + e_2 + e_3 + e_4 + e_5)\}$

Step 2. $e'' = e - a(v_0'' + v_1'') - c(v_2'' + v_3'')$

Step 3. $\tilde{v} = v'' - w(e_0'' + e_1'' + e_2'' + e_3'' + e_4'' + e_5'')$
 $-u(e_6'' + e_7'' + e_8'' + e_9'' + e_{10}'' + e_{11}'')$

Step 4. $\tilde{e} = e'' - s(\tilde{v}_0 + \tilde{v}_1) - r(\tilde{v}_2 + \tilde{v}_3).$

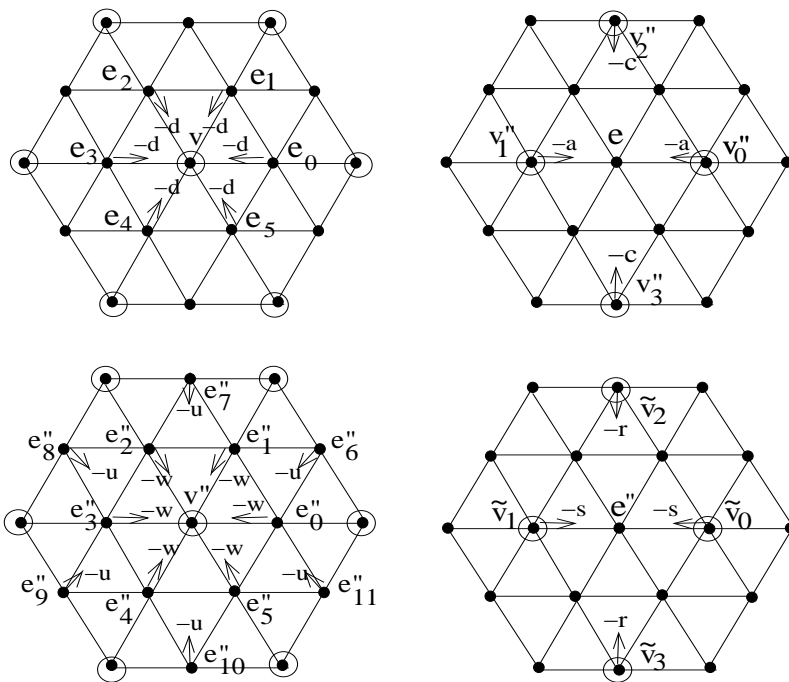


Figure 12: *Top-left: Decomposition Alg. Step 1; Top-right: Decomposition Alg. Step 2; Bottom-left: Decomposition Alg. Step 3; Bottom-right: Decomposition Alg. Step 4*

Reconstruction Algorithm:

Step 1. $e'' = \tilde{e} + s(\tilde{v}_0 + \tilde{v}_1) + r(\tilde{v}_2 + \tilde{v}_3)$

Step 2. $v'' = \tilde{v} + w(e''_0 + e''_1 + e''_2 + e''_3 + e''_4 + e''_5)$
 $+u(e''_6 + e''_7 + e''_8 + e''_9 + e''_{10} + e''_{11})$

Step 3. $e = e'' + a(v''_0 + v''_1) + c(v''_2 + v''_3)$

Step 4. $v = bv'' + d(e_0 + e_1 + e_2 + e_3 + e_4 + e_5)$.

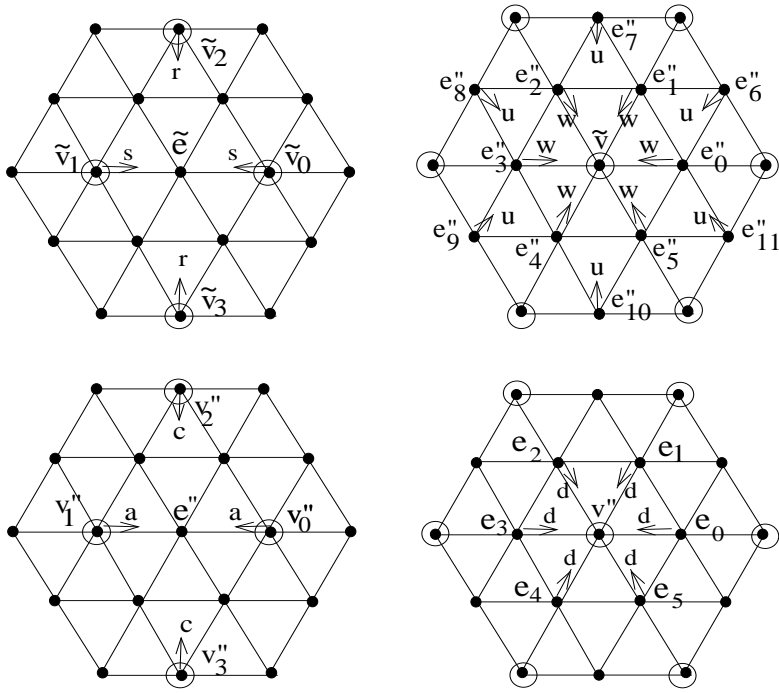


Figure 13: *Top-left: Reconstruction Alg. Step 1; Top-right: Reconstruction Alg. Step 2; Bottom-left: Reconstruction Alg. Step 3; Bottom-right: Reconstruction Alg. Step 4*

Thanks for your attention!